Springer

Acta Mechanica Sinica

CrossMark click for updates

• RESEARCH PAPER •

Acta Mech. Sin., Vol. 41, 324069 (2025)
https://doi.org/10.1007/s10409-024-24069-x

Numerical evaluation of a new high pressure water jet interference method for bridge pier protection against vessel collision

Jincai Chen[1,2], Xiquan Wei[1], Jingjing Huang[1], Ding Fu[1], Haibo Wang[1*], and Zhideng Zhou[2]

[1] *School of Civil and Transportation Engineering, Guangdong University of Technology, Guangzhou 510006, China;*
[2] *The State Key Laboratory of Nonlinear Machanics, Institute of Mechanics, Chinese Academy of Sciences, Beijing 100190, China*

Received April 20, 2024; accepted May 8, 2024; published online June 18, 2024

Ship-bridge collisions happen from time to time globally, and the consequences are often catastrophic. Therefore, this paper proposes a new high-pressure water jet interference (HPWJI) method for bridge pier protection against vessel collision. Unlike traditional methods that absorb energy by anti-collision devices to mitigate the impact force of ships on bridges, this method mainly changes the direction of ship movement by lateral high-pressure water jet impact, so that the ship deviates from the bridge piers and avoids collision. This paper takes China's Shawan River as the background and simulates the navigation of a ship (weighing about 2000 t) in the HPWJI method in the ANSYS-FLUENT software. The simulation results show that the HPWJI method has a significant impact on the direction of the ship's movement, enabling the ship to deviate from the pier, which is theoretically feasible for preventing bridge-ship collisions. The faster the ship's speed, the smaller the lateral displacement and deflection angle of the ship during a certain displacement. When the ship speed is less than 7 m/s, the impact of water flow on the ship's trajectory is more significant. Finally, this paper constructs a model formula for the relationship between the lateral displacement and speed, and surge displacement of the selected ship. This formula can be used to predict the minimum safe distance of the ship at different speeds.

Ship-bridge collision, Anti-collision device, Water jet, Safe distance

Citation: J. Chen, X. Wei, J. Huang, D. Fu, H. Wang, and Z. Zhou, Numerical evaluation of a new high pressure water jet interference method for bridge pier protection against vessel collision, Acta Mech. Sin. **41**, 324069 (2025), https:// doi.org/10.1007/s10409-024-24069-x

1. Introduction

Ship-bridge collision accidents are far from rare globally. Especially, with the rapid economic development of China, the demand for transportation of passengers and goods, as well as the freight transportation by river vessels, is constantly growing. The transport routes of river vessels are becoming more and more dense, and the number of bridges is also growing exponentially [1]. This results in an increased probability of collisions between ships and bridges [2, 3]. Once ship-bridge collision accidents occur, the consequences are often catastrophic and need to be taken seriously. Currently, the issue of ship-bridge collision has become an important research field at the international level, and the research on ship-bridge collision prevention devices or methods is a hotspot in this field.

Scholars at home and abroad have made relatively rich achievements in the research of collision avoidance devices/methods. These devices/methods can be roughly divided into active collision avoidance and passive collision avoidance from the collision prevention mode [4]. The former refers to the intervention of ship navigation management and trajectory to reduce the probability of ships colliding with bridges and avoid the occurrence of serious ship-bridge collisions. The latter utilizes anti-collision devices to absorb the kinetic energy of ships and reduce the impact force of ships on bridges.

Wang et al. [5,6] used the complementarity of infrared and

*Corresponding author. E-mail address: wanghaibo@gdut.edu.cn (Haibo Wang)
Executive Editor: Yue Yang

visible light imaging detection to establish an active early warning system for preventing ship collisions with bridges, and proposed a track prediction Kalman filtering method based on multi-feature adaptive fusion tracking. Ma et al. [7] proposed a new ship-bridge collision probability formula that takes into account different safety measures. Tran et al. [8] wrote a set of active collision avoidance algorithms that enable ships to detect collision threats caused by changes in the heading of nearby ships. Both active and passive safety measures can effectively reduce the probability of ship-bridge collisions. If properly deployed, active measures can provide the same level of protection as passive measures.

In passive collision protection, to mitigate the impact of ships on bridges, researchers have conducted extensive research on the materials and composition of collision protection devices. For example, Mei et al. [9,10] studied the high-speed impact response mechanism of composite sandwich panels with glass fiber reinforced plastic (GFRP) prismatic core materials based on numerical simulation; Ehlers et al. [11] used nonlinear finite element method to analyze the impact resistance of X-core structures and verified it through experiments; Lian et al. [12] investigated the energy absorption characteristics of circular paper tubes under axial loads, proposed a simplified circular paper tube spiral multi-leaf folding mode, and established a theoretical prediction model for the energy absorption performance of circular tubes under impact. With the continuous development of new materials science, Zhu et al. [13, 14] and Tian [15] proposed a large-scale composite new bumper system. The system module is mainly composed of GFRP, polyurethane (PU) foam core material and ceramic particles. This type of device has excellent corrosion resistance and self-floating properties, and has high installation efficiency on site. In order to protect both bridge piers and ships, flexible collision protection devices are often used in bridge design, and numerical simulation is used to study the mechanical properties of the devices under impact loads [16-19].

In summary, the active collision avoidance method provides collision risk warning, allowing ships to take measures in advance to avoid collisions with bridges or to mitigate impact forces; passive collision avoidance uses collision avoidance devices to absorb the kinetic energy of ships when they are about to hit bridge piers, reducing the impact of ships on bridges. The combined use of these two methods may provide more comprehensive protection for both ships and bridges. However, current research on passive collision avoidance mainly focuses on absorbing the kinetic energy of ships through frontal interception to mitigate impact on bridges, and there is little research on avoiding collisions by diverting ships' energy through changing the ship's trajectory. This article proposes a new high-pressure water jet interference (HPWJI) method for bridge pier protection against vessel collision from the perspective of fluid dynamics. By setting up high-power jet sources near bridge piers, fluid is used to change the direction of ship movement to protect the bridge piers. This article mainly explores the feasibility of this anti-collision method through numerical simulation, providing new ideas and perspectives for the development of ship-bridge anti-collision devices.

2. HPWJI method for bridge pier protection

The cargo ships sailing on the river often have large momentum. If the ship is intercepted from the front, according to the impulse theorem, the longer it takes for the ship to be intercepted, the smaller the impact force of the ship on the collision avoidance device or bridge. Therefore, most researchers use new composite materials or flexible materials to build collision avoidance devices. This article takes a different approach and plans to use high-pressure water jet impact to change the direction of ship movement, making it deviate from the pier and achieving the purpose of collision avoidance. The specific measures are as follows: Arrange large-caliber high-flow injection devices at a certain distance in front of the pier to interfere with the flow field structure, so that the ship deviates from its original direction of travel when passing through the specific flow field area, and ultimately avoids the pier. Whether this method is feasible involves the coupled interaction of many parameters, such as ship tonnage, ship speed, water speed, high-pressure water flow rate, and location of the water jet. The mutual influence law between these parameters will be discussed in this article and in our subsequent research.

3. CFD simulation analysis

3.1 Geometric model and computational domain

This paper takes the Shawan river channel in China as the basin background. The common water velocity in this basin is about 1.5 m/s. The typical ships in this basin weigh about 2000 t. The ship model selected for this study is 74 m long, 11 m wide, 6.4 m deep, 3 m in draft, and weighs 2139 t, and the geometric model is shown in Fig. 1.

In order to investigate the relationship between the ship speed, deflection angle, surge displacement (displacement along the river line) and transverse displacement (displacement perpendicular to the river line) of a selected ship under the influence of a fixed high-pressure water jet, this paper selects a high-pressure water jet nozzle with a diameter of

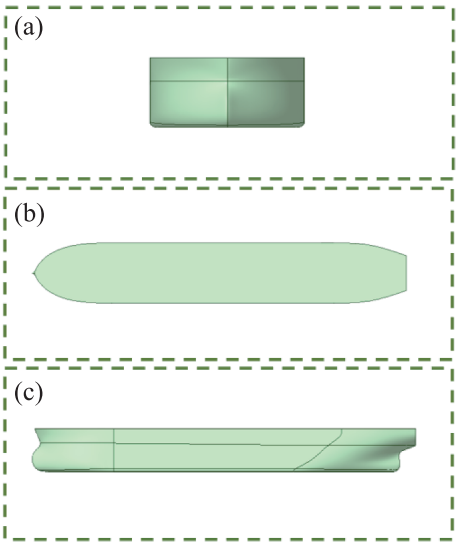

Figure 1 Geometric model of the ship. (a) The plan view of the bow; (b) the plan view of the whole ship; (c) the side view of the hull.

2 m [20], with the nozzle mouth flush with the water surface, a water jet flow rate of 32 m^3/s, and a vertical distance of 4 m from the water outlet to the ship's navigation line. The length, width and height of the calculation domain are set to 300 m × 110 m × 64 m, and the overall schematic diagram is shown in Fig. 2.

3.2 Numerical method and boundary conditions

Currently, the engineering problems of ships and ocean structures solved by computational fluid dynamics are mainly based on the Reynolds-averaged Navier-Stokes (RANS) method [21]. Therefore, this article selects the RANS k-ω shear stress transfer model to solve the turbulence field, in which the velocity and pressure coupling are iteratively solved by the SIMPLE algorithm. The discretization of the convective and diffusive terms uses a second-order upwind difference format and central difference format, respectively. The multiphase flow model selects the VOF (volume of fluid) model to perform interface tracking. The inlet of the computational domain is a mixed velocity inlet of air and liquid, and the incoming velocity is defined using a submodel of VOF called the open channel wave boundary. The outlet is a pressure outlet. The upper side and the left and right sides of the basin can be regarded as infinite extension of the flow field, so symmetric boundary conditions are used. The remaining components are set as no-slip walls.

Through the DEFINE_SDOF_PROPERTIES macro in the UDF, the corresponding mass and rotational inertia on each axis can be specified for the hull. After defining the mass and rotational inertia of the hull, the six-degree-of-freedom system can be used to solve the motion state of the ship at each moment. To simulate the scene of the ship moving towards the pier at a constant speed, this paper sets the speed of the ship as a constant.

3.3 Mesh division and validation

The overlapping grid technology is adopted to divide the grids of the ship and fluid calculation domain respectively. The main grid adopts the polyhedron grid, and the local grid is intensified near the water surface and around the ship's route. In order to ensure the accuracy of the grid, this article generates five sets of grids with different sizes. The detailed parameters can be seen in Table 1, and the grid independence is verified by simulating the surge displacement of freely floating ships under only water force [22-24].

Figure 3 shows the time-varying curve of the ship's surge displacement when it is freely floating and only affected by water force. It can be found from the figure that when the minimum grid size is larger than 0.5 m, the surge displacement curves of different numerical examples are quite different, and the calculation results are greatly affected by the grid size. When the minimum grid size is less than 0.5 m, the differences of surge displacement curves have become very small. Moreover, with the decrease of minimum grid size, the calculation results gradually tend to be on the same curve.

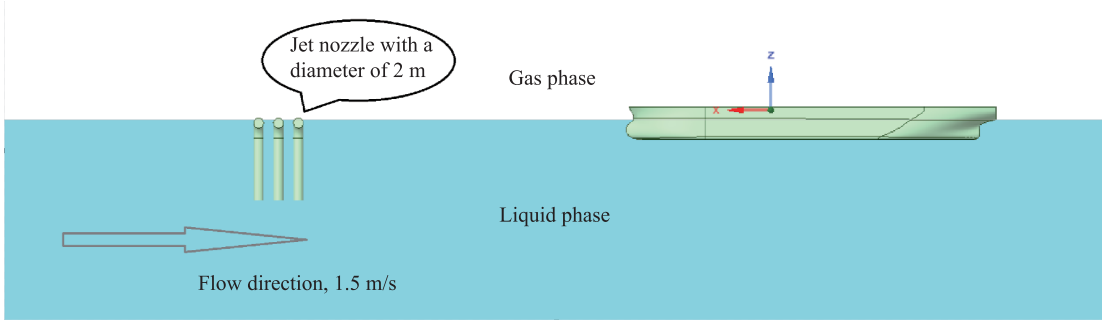

Figure 2 Schematic diagram of the high-pressure water jet nozzle and computational domain.

Table 1 Basic parameters for different grids

Minimum grid size (m)	Total number of volume grids (million)	Total number of face grids (million)
0.60	0.65	4.43
0.55	0.95	6.46
0.50	1.30	9.00
0.46	1.50	10.19
0.43	1.65	11.18

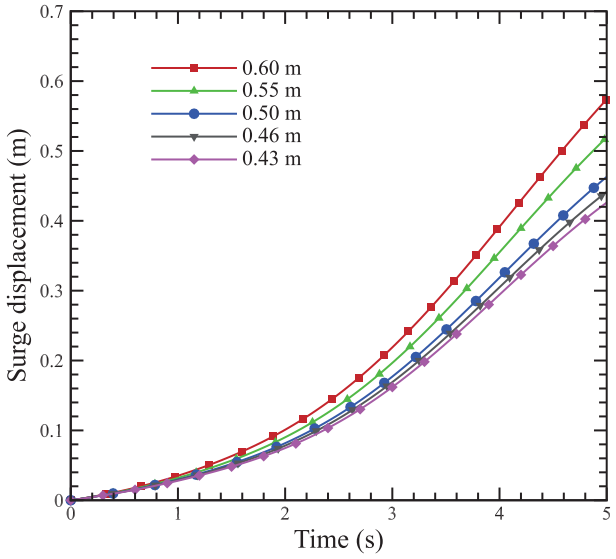

Figure 3 Time-varying curve of the ship's surge displacement when it is freely floating and only affected by water force under different grids.

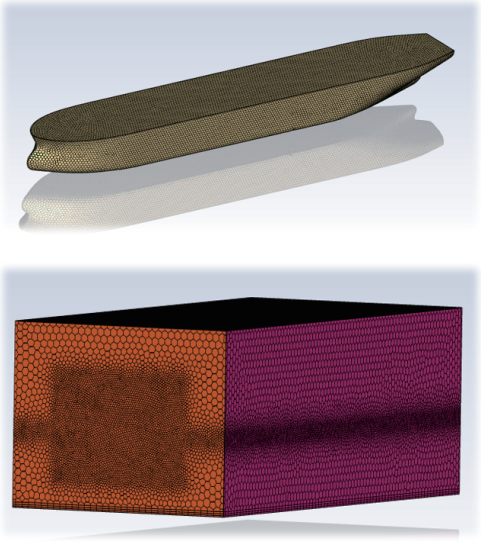

Figure 4 Schematic diagram of the ship and computational domain grid partition.

Taking into account both calculation accuracy and efficiency, this paper finally selects the fourth set of grid for subsequent calculations. The minimum grid size of this grid is 0.46 m, and the maximum grid size is 3.6 m. The grids of ship body and computational domain are shown in Fig. 4.

3.4 CFD model verification

To validate the reliability of the CFD model, this study constructed an experimental wave-making pool identical to the one at the Applied Mechanics Research Institute of Kyushu University [25] during the simulation process. The specific dimensions of this wave-making pool are: 18 m in length, 0.3 m in width, and 0.7 m in height. One end of the pool is equipped with a plunging-type wave generator, while the other end is installed with a wave absorber. A convex float was set up 7 m away from the wave-making end to study the influence of different wave forms on its pitch and roll. In this model validation, we adopted the same numerical methods as previously described. At the inlet of the wave-making pool, numerical wave generation was set up, and numerical wave elimination was conducted at the outlet. The wavelength in the experiment was set to 1.476 m, and the wave height was 0.062 m. To obtain accurate numerical results, we selected data from the 20th to 25th seconds of the tail section for comparative analysis. As shown in Fig. 5, it was found that these results are basically consistent with the pitch (Fig. 5(a)) and roll (Fig. 5(b)) results caused by combined waves in the Zhao's experiment [25], with good data agreement, thus validating the reliability of the CFD model in this study.

4. Numerical results

4.1 High-pressure water jet impact region

The high-pressure water jet has an initial velocity direction perpendicular to the ship's direction of travel, generating a lateral thrust on ships passing nearby, thereby changing their direction of travel. Therefore, this article considers the region where the lateral velocity of water flow near the high-pressure water jet is greater than 0.3 m/s [26] as the impact

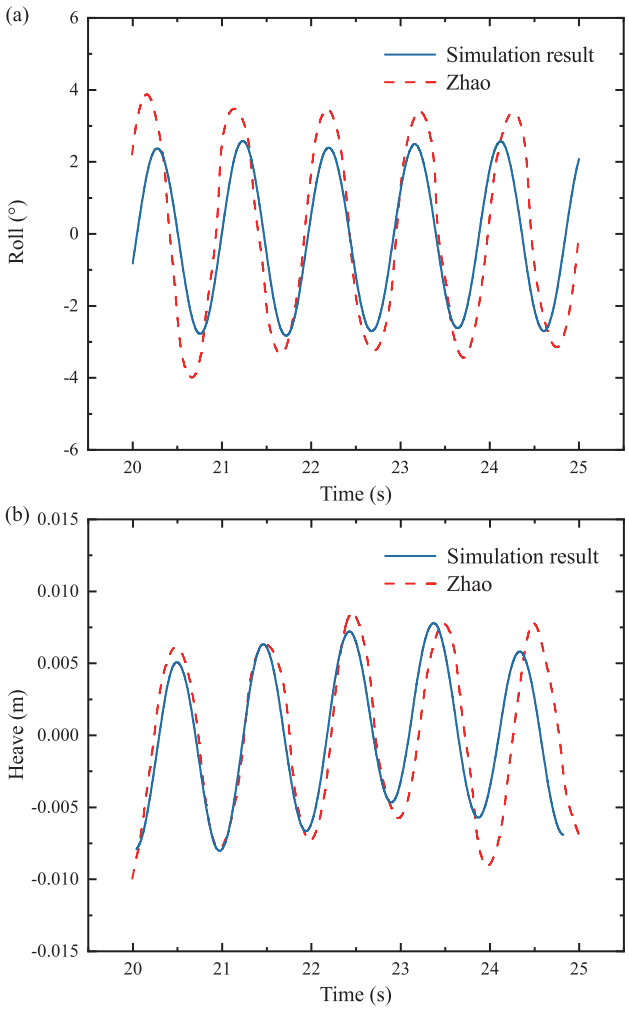

Figure 5 Comparative verification with Zhao's experiment [25]: (a) pitch of the convex float; (b) roll of the convex float.

region of the high-pressure water jet. Figure 6(a) and (b) show the contours of the water horizontal velocity and dynamic pressure within the impact region of the high-pressure water jet. It can be found from Fig. 6(a) that the impact region of the water jet starts at the nozzle and expands like a scallop shape. The horizontal velocity is maximum at the nozzle, reaching approximately 10 m/s, where the corresponding dynamic pressure is also maximum, reaching 44,900 Pa. The end of the impact region is slightly inclined towards the downstream due to the initial water flow, and the impact range is about 21 m from the nozzle.

In order to further discuss the effect of the high pressure water jet on the ship's steering, this paper divides the region near the water jet into four zones according to the change of water kinematic energy, named S1, S2, S3 and S4 as shown in Fig. 7(a). The distribution of water kinematic energy in each zone is shown in Fig. 7(b). Among them, S1 is the high-energy impact zone, which has the greatest impact on ship steering. The impact range is about 7.5 m, and within this range, the water kinetic energy decreases rapidly in an exponential form. S2 is the medium-energy impact zone, with an impact range of about 7.5 m. The curve of water kinetic energy is convex, and the energy decrease speed slows down. S3 is the low-energy impact zone, with an impact range of about 6 m. The change of water kinetic energy is relatively gentle. S4 is the invalid zone, and the impact on the ship when it is driving in this area can be ignored. S1-S3 are effective water jet impact zones. When the ship passes through this area, the original motion attitude of the ship will be interfered, so as to reduce or avoid the impact of the ship on the bridge pier. It can be called "bridge pier protection zone".

4.2 The influence of high pressure water jet on ship motion

In the process of ship navigation, the setting position of high-pressure water jet has an important impact on the ship's nav-

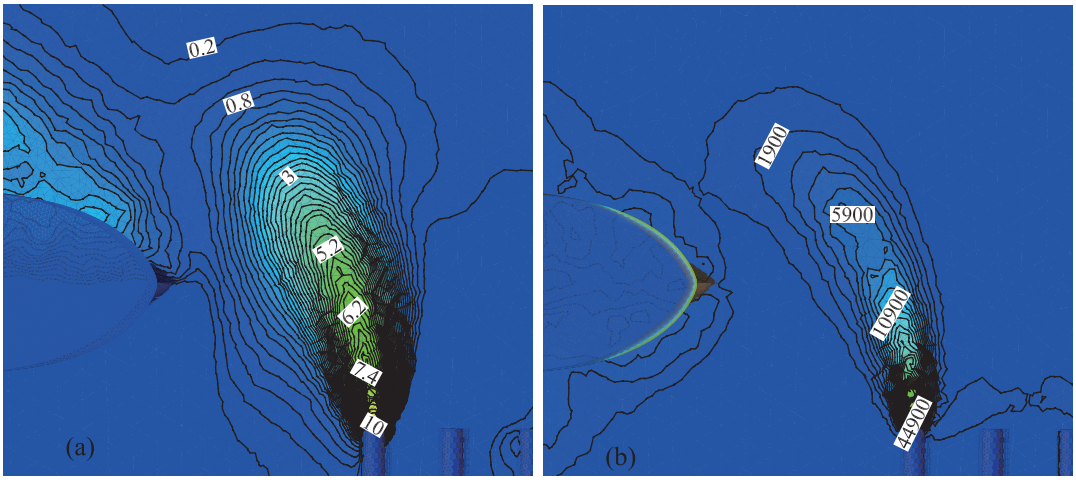

Figure 6 The flow field of the region affected by the high pressure water jet. (a) Horizontal velocity contour; (b) dynamic pressure contour.

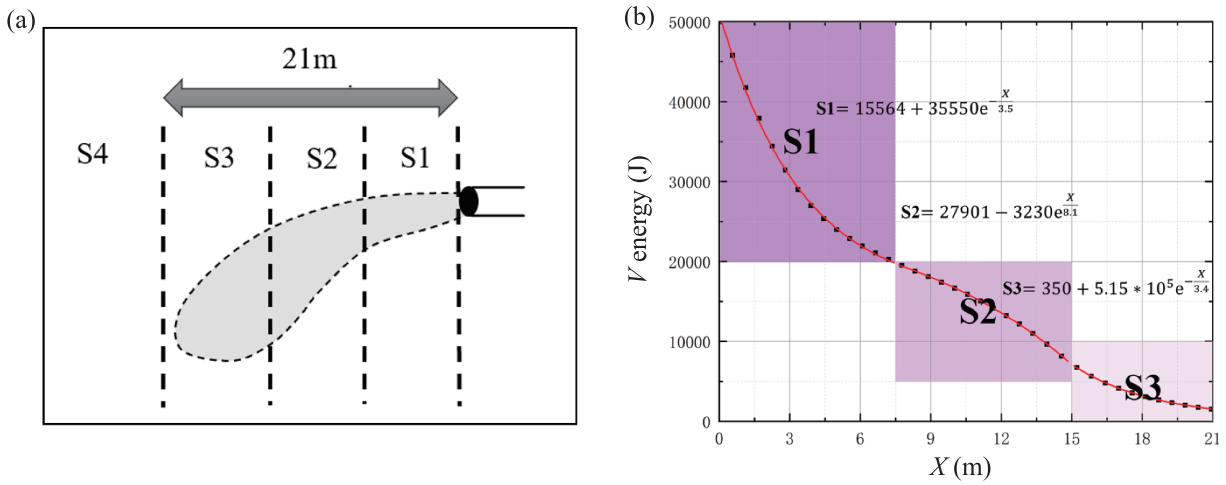

Figure 7 (a) The impact region of high pressure water jet; (b) the kinetic energy variation curve of water flow in each zone.

igation status. The high-pressure water jet mentioned in this article is set at a distance of 4 m from the ship's central line. When the ship is traveling upstream, it will directly encounter the high-energy impact area S1. In this area, the ship will not only be subject to the lateral impact force of the water jet, but also change the flow field structure within this area. The change of flow field structure means that the dynamic characteristics and flow patterns of water flow will change, which further affects the ship's navigation status. Figure 8 shows the water velocity contour and dynamic pressure contour when the bow of the ship arrives at the jet nozzle (Fig. 8(a), (d), and (g)), when the bow passes over the jet nozzle (Fig. 8(b),

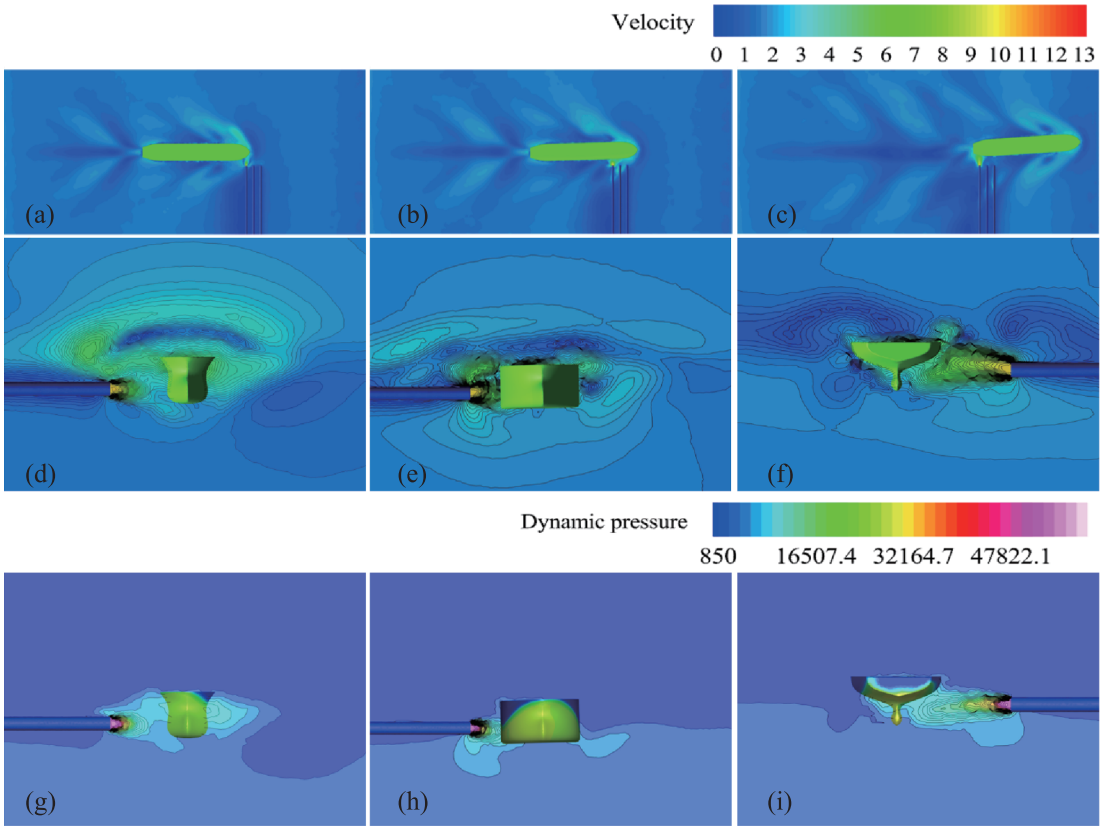

Figure 8 Water flow field around a ship as its bow enters and its stern exits the impact zone S1. (a) The bow just reaches S1; (b) the bow fully enters S1; (c) the stern exits S1; (d) water velocity contour in (a); (e) velocity contour in (b); (f) velocity contour in (c); (g) dynamic pressure contour in (a); (h) dynamic pressure contour in (b); (i) dynamic pressure contour in (c).

(e), and (h)), and when the stern exits the jet nozzle (Fig. 8(c), (f), and (i)). It can be observed from the figure that as the bow passes through the jet mouth, the water flow velocity on the left side of the ship's forward direction decreases significantly, indicating that the bow has passed through the high-pressure water jet area. At the same time, the pressure in this area drops sharply, showing rapid changes in fluid dynamics. On the right side of the ship's forward direction, we can see that the pressure has increased. This asymmetric pressure distribution causes a lateral force, which prompts the ship to turn to the left. This turning trend is further reflected in the velocity contour, where the water velocity on the right side is significantly higher than on the left, exacerbating the ship's turning effect. As the ship continues to move forward, the turning angle on the left side of its forward direction gradually increases, leading to further decreases in water velocity and pressure on that side. When the stern finally reaches the jet nozzle, the difference in fluid pressure between the left and right sides of the ship becomes particularly significant, with the dynamic pressure on the right side of the forward direction being much higher than on the left. Although theoretically, when the water jet impacts the ship's hull beyond its center of gravity, it may cause a decrease in the ship's forward turning angle, in practice, once the ship's turning angle reaches a certain degree, the gradually increasing pressure difference between the left and right sides begins to dominate the turning process, causing the ship to continue turning to the left of its forward direction, and the turning angle continues to increase. This increase and change of flow velocity have a significant impact on the ship's navigation performance and hull dynamics. High-speed water flow can generate impacts, potentially damaging the hull structure, increasing the ship's resistance, thereby affecting its speed of navigation.

However, considering that the high-pressure water jet speed involved in this article is relatively low, with a maximum value of only 10 m/s, and the water jet does not directly impact the ship's hull but indirectly affects its sailing by pushing the water between the jet nozzle and the ship, a preliminary analysis is conducted in this article to assess the force on the ship's structure caused by the high-pressure water jet. When the water jet ejects from the high-pressure nozzle and reaches the mid-section of the ship's hull, the maximum pressure generated is about 28685 Pascals. In order to assess whether the strength of the ship meets the established requirements, this paper constructs an ideal simply supported beam model for calculation and analysis. The model sets the beam length to 3.6 m (consistent with the spacing of the actual ribs), the width to 1 m (unit length), and the thickness to 0.05 m [27]. It is subjected to a uniform vertical distributed force of 30,000 Pascals. By applying the principles of material mechanics, we calculated that the maximum tensile stress of the plate is approximately 58 MPa. However, considering that the steel plate at this position in the actual situation belongs to a statically indeterminate structure, the model may overestimate the stress value. In addition, this calculated stress value is far lower than the yield strength of 235 MPa for commonly used strength steel in ship hulls [27]. Therefore, this paper currently does not consider the potential impact of water columns on the ship's structure and will further discuss it in subsequent research on water column strength.

When the bow of the ship encounters the water jet, it causes large waves with a height even close to the top of the ship. These large waves adhere to the bow position, exerting significant effects on the drag of the hull. Specifically, they mainly affect wave resistance and viscous resistance [28]. Wave resistance is generated by water waves produced when the hull is propelled, while viscous resistance is generated by the viscous force of water molecules on the hull surface. The formation and adherence of these waves not only increase the drag on the ship, leading to a decrease in ship speed, but also help to reduce potential damage to structures such as bridge piers.

Figure 9 shows the changes in resistance of ships near the jet. In the figure, the horizontal axis represents the distance from the ship's center of gravity to the jet nozzle. Negative values indicate that the ship is downstream of the jet nozzle, while positive values indicate upstream. The vertical axis reflects the magnitude of resistance on the hull. The dashed line corresponds to an x-coordinate of approximately –37 m, indicating that the ship's center of gravity is located 37 m

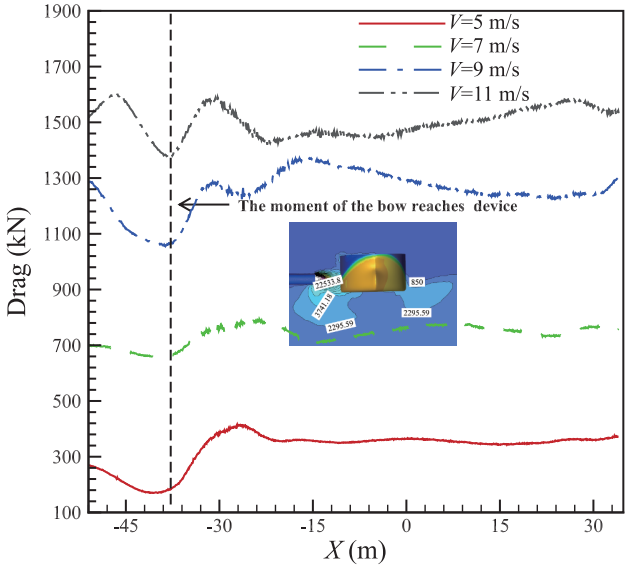

Figure 9 Resistance variation curves of ships with different initial velocities near the jet.

downstream of the jet nozzle, where the bow of the ship just reaches the jet nozzle. When x = 0 m, the ship's center of gravity is exactly at the jet nozzle; and when x = 37 m, the stern of the ship will pass through the jet nozzle.

It is evident from Fig. 9 that once the bow passes through the jet nozzle, the resistance of the ship under different speed conditions increases significantly. After some time, there is a brief spike in resistance, which is caused by changes in fluid structure and the ship's motion becoming unstable due to different moments acting on it. However, as the bow continues to pass through the jet nozzle, the disturbance caused by the jet water column on the waves rising from the water surface leads to a gradual stabilization of the ship's resistance throughout the entire process, from the middle of the ship to the position of the nozzle, and then to the stern exiting the nozzle.

Moreover, during the navigation of a ship, it generates waves, leading to the phenomenon of heave. The amplitude of heave has a direct impact on the stability of the ship's movement and the comfort of passengers. Figure 10 shows the heave variation curves of ships with different initial speeds under upstream conditions. As can be seen from the figure, as the speed of the ship increases, the amplitude of heave also increases accordingly. Before the ship enters the water jet impact area (i.e., at a position where x is less than –37 m), when the ship's speed is 5 m/s, the amplitude of heave is the smallest. At this point, the difference between the peak and trough of the wave is only 0.25 m, and the wavelength is approximately 30 m. However, when the ship's speed increases to 11 m/s, the amplitude of heave reaches its maximum, with a peak-to-trough difference of up to 0.57 m and a wavelength of approximately 60 m. Notably, regardless of the ship's speeds, once it enters the water jet impact area, the amplitude of heave decreases. At a speed of 5 m/s, the fluctuation difference decreases significantly, with a minimum amplitude of only 0.06 m and a wavelength of approximately 26 m. On the other hand, at a speed of 11 m/s, the minimum amplitude of the fluctuation difference is approximately 0.2 m, and the wavelength is approximately 56 m. This phenomenon occurs primarily because the water jet emitted from the high-pressure jet nozzle disturbs the waves generated by the ship's bow, effectively reducing the amplitude of heave.

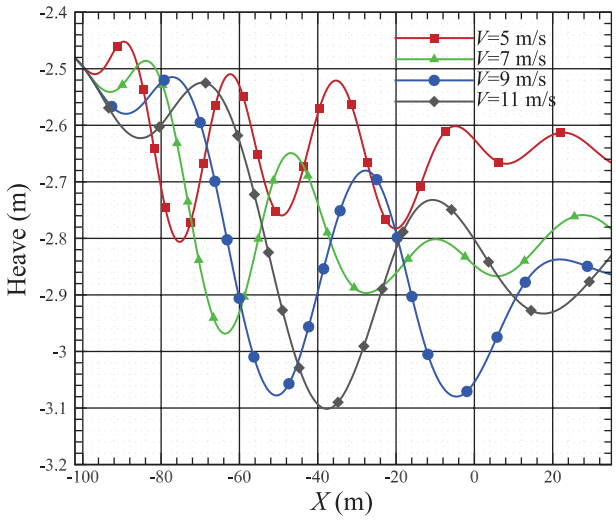

Figure 10 Heave curves of ships with different initial speeds under upstream conditions.

4.3 The effect of initial velocity on ship yaw

When the ship has not yet started, the water is in a stationary and undisturbed state. Derradji Aouat and Earle [29] pointed out that changes in the ship's velocity significantly disturb the fluid, affecting the stability of the ship's motion attitude and the accuracy of the calculated results. Song et al. [23] believed that it is necessary to simulate the fluid-structure interaction of ships by driving a certain distance to generate stable bow waves. In this study, the ship is placed 70 m away from the jet, and moves forward at a constant initial velocity before interacting with the water jet, in order to obtain a more realistic and reasonable ship motion. Four groups of initial velocity conditions are set in this study, namely 5, 7, 9, and 11 m/s. Figure 11 shows the motion trajectory of ships under different initial velocity conditions from top to bottom in each row. It can be seen from Fig. 11 that the wave pattern of the ship during navigation is consistent with the Kelvin wave pattern in actual ship navigation. The larger the initial velocity of the ship, the smaller the Kelvin angle and the smaller the deflection angle of the bow.

In the previous research, this article only discussed the working condition group of ships moving upstream with a water flow velocity of 1.5 m/s. In order to distinguish the impact of upstream and downstream flow on numerical simulation results, this article has set a working condition group of downstream flow with the same water velocity of 1.5 m/s. Figure 12 shows the ship's trajectory after passing through the high-pressure water jet area. Figure 12(a) is the upstream working condition group, and Fig. 12(b) is the downstream control working condition group. As shown in Fig. 12, whether upstream or downstream, ships with different initial velocities, after passing through the high-pressure water jet area, began to deviate towards the side of the water jet spray, and the greater the initial velocity, the smaller the ship's deflection angle and lateral displacement. In the upstream condition, when the speed of the ship is 5 m/s, the lateral displacement of the ship from the bow to the stern passing through the jet nozzle is approximately 6.7 m. However, when the speed increases to 11 m/s, the lateral displace-

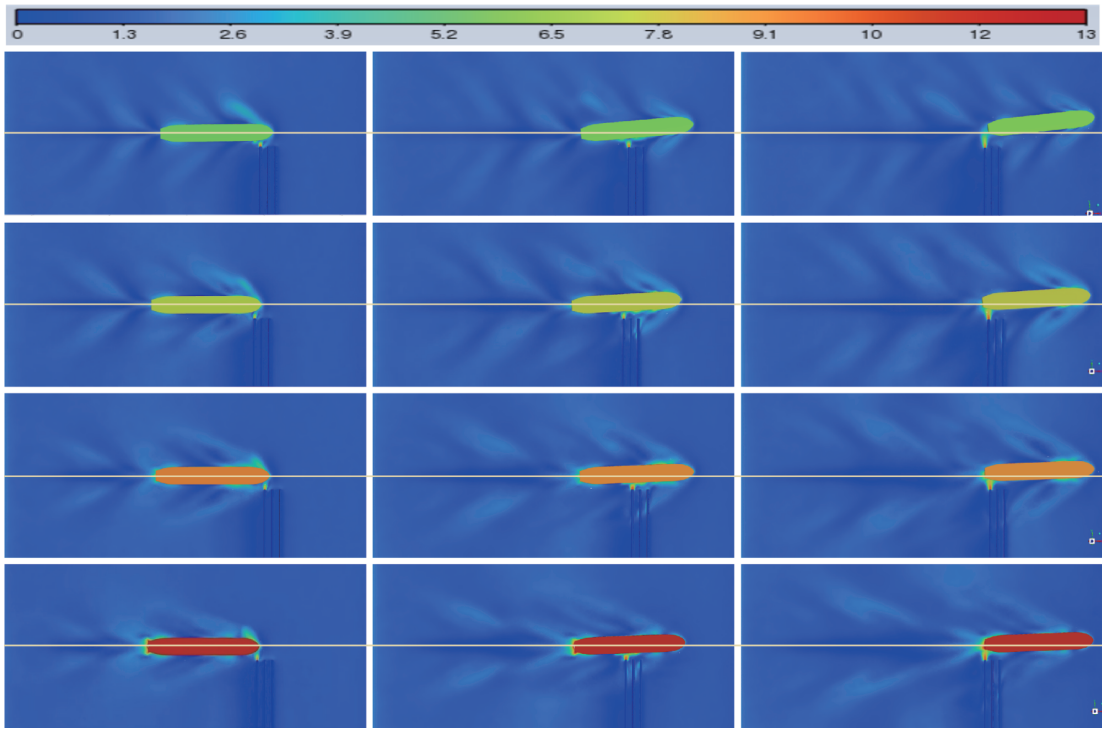

Figure 11 Ship trajectory affected by high pressure water jet with different initial velocity. The initial velocity of each row of ships from top to bottom is 5, 7, 9 and 11 m/s, respectively.

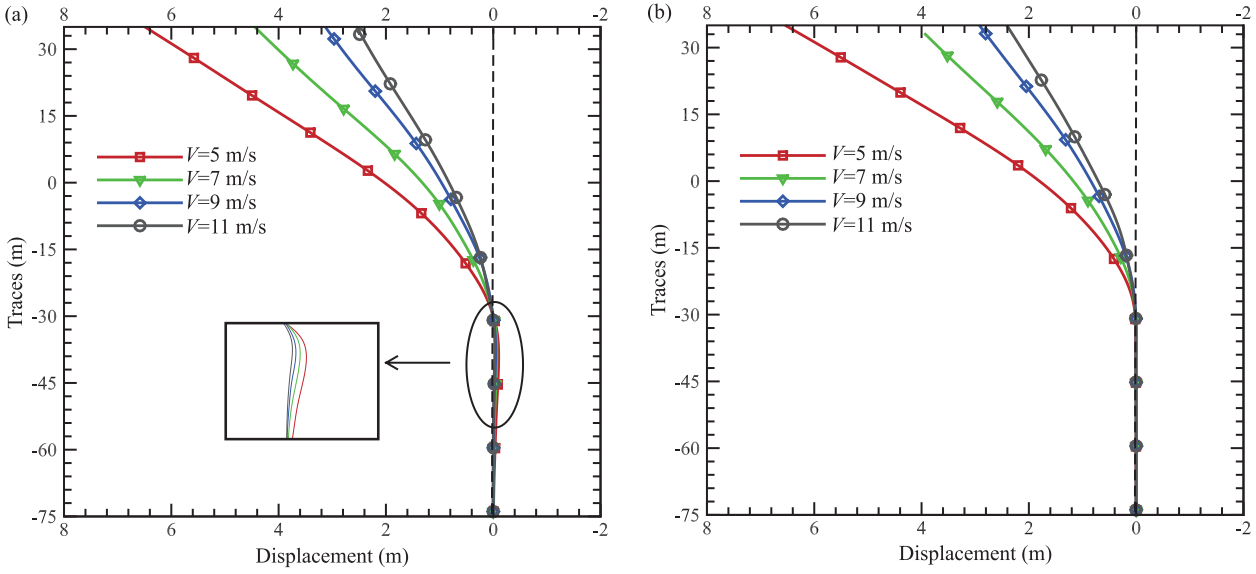

Figure 12 Ship trajectory after passing through the high pressure water jet. (a) Upstream conditions with initial ship velocity of 5, 7, 9, and 11 m/s, respectively; (b) downstream conditions.

ment of the bow is reduced to a minimum of approximately 2.4 m under the same surge displacement. Regardless of whether the ship is in a downstream or upstream condition, the lateral displacement of the ship is roughly equivalent. For example, when the initial speed of the ship is 5 m/s, the lateral displacement under the same surge displacement is approximately 6.8 m, with an error of only 1.5% compared to the upstream condition. Although downstream and upstream conditions can affect the resistance encountered by the ship, thereby altering its speed, this article simplifies the analysis by assuming a constant speed for the ship. Therefore, the impact of resistance variations on the motion of a ship traveling at a constant speed is relatively small.

The main difference between upstream and downstream

conditions is that when ships first enter the water jet impact region, the trajectory of ship's center of gravity in the upstream condition will deviate slightly towards the opposite direction of the water jet. This deviation decreases with increasing initial velocity of the ship, as shown in Fig. 12(a) in the small figure. When the bow just starts to deviate to the left due to lateral water flow, under upstream conditions, the water flow on the bow will generate an additional counterclockwise torque couple, accelerating the rotation of the ship and causing a slight rightward deviation of the ship's center of gravity. At low ship speeds, the effect of upstream flow is more pronounced, with greater reverse deviation of the ship's center of gravity. As shown in Fig. 13(a), when the bow just experiences lateral water flow, a large vortex will be generated on the left side of the ship under upstream conditions, accelerating the ship's turn. It is worth noting that despite the presence of this reverse lateral displacement phenomenon, the amount of lateral displacement is actually very small. For example, when the speed of the ship is 5 m/s, the reverse lateral displacement of its center of gravity is only 0.1 m. This minute displacement does not have a substantial impact on the normal navigation of the ship. Therefore, to simplify the discussion and highlight the main characteristics of the upstream condition, this article will focus on the analysis of the upstream condition in the subsequent content and will not repeat the relevant results of the downstream condition.

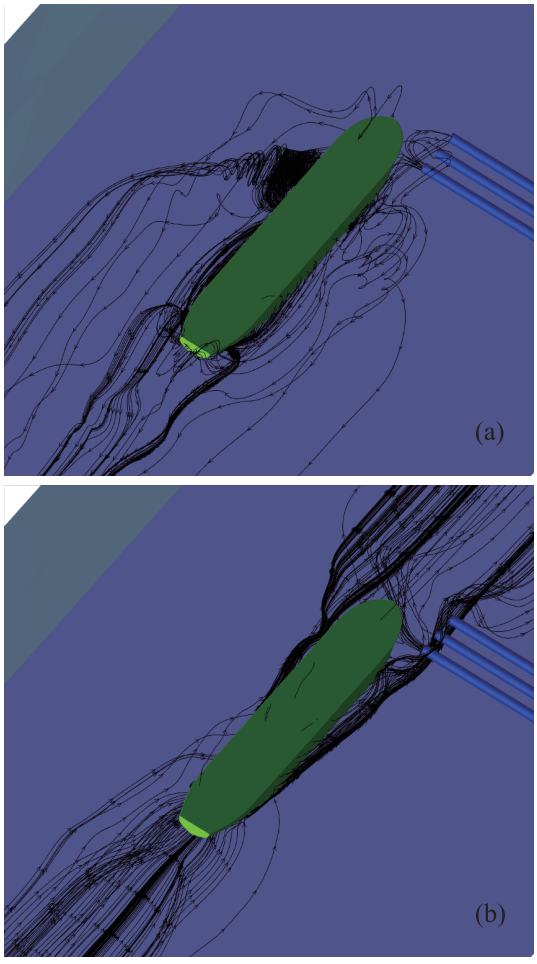

Figure 13 Water flow streamlines when the ship enters the high pressure water jet. (a) Upstream conditions; (b) downstream conditions.

According to previous research, when the ship collides with the pier head-on, the impact force is the largest, and when the ship collides with the pier sideways, the impact kinetic energy on the pier is greatly reduced [30, 31]. Therefore, if the ship cannot fully avoid the pier under the influence of high pressure water jet, the deflection angle of the ship during collision with the pier is also an important parameter affecting the impact force. This article presents the curves of deflection angle of ships with different initial velocities after passing through the high pressure water jet under upstream conditions, as shown in Fig. 14. It can be found from Fig. 14 that after passing through the high pressure water jet ($x > -37$ m), the deflection angle of the ship increases rapidly. As it gradually moves away from the water jet area, the change in deflection angle of the ship gradually slows down and finally tends to a stable value. The faster the initial velocity, the less time the ship spends in the water jet area, and the less affected by lateral water flow. Finally, the deflection angle is also smaller. For example, when the initial velocity is 5 m/s, the deflection angle of the ship is about 6.2° when the stern reaches the nozzle ($x = 37$ m). However, when the initial velocity is 11 m/s, the deflection angle of the ship is about 2.3°. Therefore, it is theoretically feasible to protect piers by setting up high pressure water jets to interfere

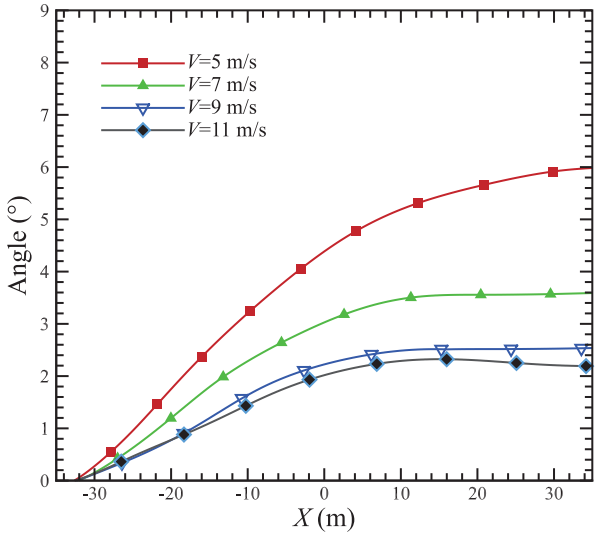

Figure 14 Curves of the deflection angle of ships with different initial velocities passing through the high-pressure water jet under upstream conditions.

with water flow and steer ships away from collision. This method is especially effective for low-speed ships, which can completely avoid piers under water jet influence and achieve "zero damage". Even for high-speed ships, they can also reduce the impact force on piers by changing the impact angle of ships.

As shown in the previous analysis, the ship is deflected to one side under the transverse flow impact of high pressure water jet. The lateral displacement of the ship increases with the increase of its surge displacement. The deflection angle first increases and finally reaches a stable value. Both the lateral displacement and the deflection angle play a positive role in protecting the pier. In addition to the initial velocity of the ship, the surge displacement in the ship's advancing direction is also a key influencing factor: if the ship has advanced a certain surge displacement, and its lateral displacement can just avoid the pier, then the surge displacement at this time can be called the minimum safe distance for ship-bridge collision prevention. That is, if the high pressure water jet is set outside the minimum safe distance, the ship can perfectly avoid the pier. In order to obtain the corresponding safe distance of ships with different initial velocities, this article obtains a relationship model between ship lateral displacement and initial velocity and surge displacement based on machine learning algorithm. The equation could be expressed as

$$\begin{aligned} Z =& 0.954 + 0.2199V + 0.1103X - 0.01153V^2 - 0.02693VX \\ &+ 0.002222X^2 + 0.001421XV^2 - 0.0000814VX^2, \end{aligned} \quad (1)$$

where Z represents the lateral displacement of the ship, V represents the initial velocity of the ship, and X represents the surge displacement of the bow after passing through the water jet. Figure 15 is an isobath map of ship lateral displacement with respect to initial velocity V and surge displacement X. Each contour line corresponds to the safe distance X under different initial velocities V of ships with a given pier width Z.

5. Conclusions

Ship-bridge collision accidents are not rare globally, although their frequency is far lower than that of terrestrial traffic accidents. However, every ship-bridge collision accident may have catastrophic consequences. This not only poses a serious threat to people's lives, but also leads to huge property losses. What's worse, such accidents often cause irreversible damage to the environment, such as water pollution and ecological damage. Therefore, we must attach great importance to the ship-bridge collision problem, strengthen prevention measures, and reduce the possibility of its occurrence.

To prevent ship-bridge collisions, this article proposes a new high-pressure water jet method for bridge pier protection against vessel collision. This method differs from traditional anti-collision devices, as it does not rely on energy absorption to reduce the impact force of the ship on the bridge. HP-WJI method directly or indirectly changes the ship's trajectory by using the lateral impact force of the high-pressure water jet, causing it to naturally deviate from the pier and avoid collision.

This article takes the Shawan river channel in China as the background, and uses ANSYS-FLUENT software to sim-

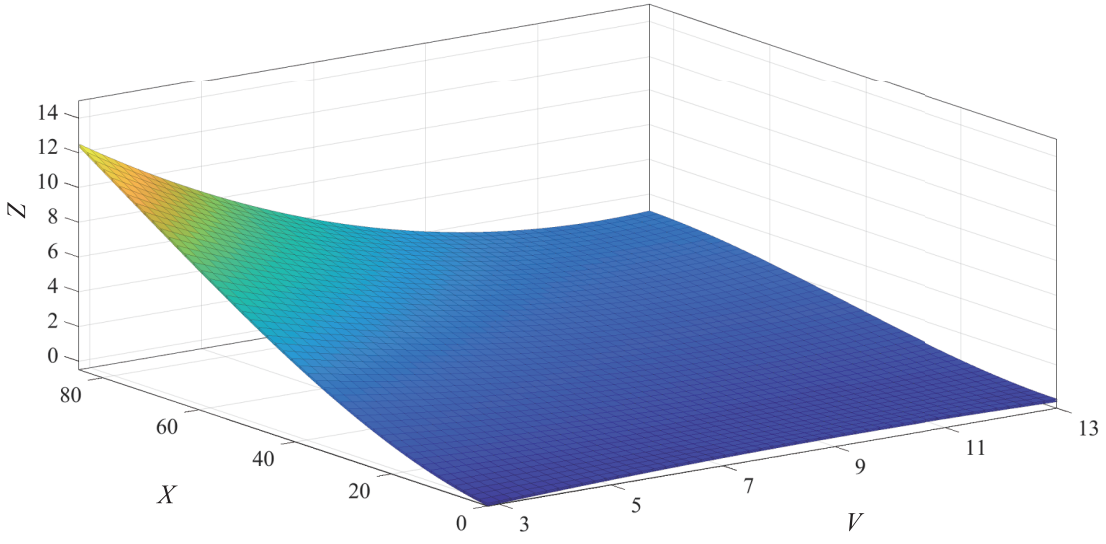

Figure 15 Contour of ship lateral displacement with respect to initial velocity (V) and surge displacement (X).

ulate the navigation of a selected ship under the HPWJI method. The simulation results show that the HPWJI method has a significant impact on the navigation direction of the ship. Specifically, the lateral impact of the high-pressure water jet can effectively change the ship's trajectory, causing it to naturally deviate from the pier, and thus effectively prevent bridge-ship collisions in theory. This result not only demonstrates the feasibility of the HPWJI method, but also provides a solid theoretical foundation for practical applications.

In the simulation, we observed that the ship's speed has a significant impact on its navigation performance under HPWJI. As the ship speed increases, the lateral displacement and deflection angle of the ship gradually decrease when traveling the same distance. It is particularly noteworthy that when the ship speed is below 7 m/s, the impact of water flow on the ship's trajectory is particularly significant. This finding reveals the limitations of the HPWJI method in practical applications and provides a new perspective for optimizing this method. After further research, this article constructs a mathematical model of the relationship between the ship lateral displacement and speed, and surge displacement. This formula can effectively predict the minimum safe distance required for typical ships at different speeds. This distance refers to the distance that the ship needs to deviate from the pier just enough with the help of the HPWJI method. The establishment of this model not only provides an accurate prediction tool for practical applications, but also provides more scientific guarantees for ship navigation safety.

In summary, the innovative anti-collision method proposed in this article is not only effective, but also does not cause damage to ships and bridges, providing a new solution for the safety of water transportation. In the future, HPWJI method is expected to become a widely used ship collision avoidance technology, ensuring the safety and smoothness of water transportation.

Conflict of interest *On behalf of all authors, the corresponding author states that there is no conflict of interest.*

Author contributions *Jincai Chen conceptualized and designed the research, authored the manuscript, and oversaw its revisions. Xiquan Wei contributed significantly to the development of the model, experimental setup, data processing, and drafted the initial manuscript. Jingjing Huang was responsible for conducting the experimental validations and analyzing the data. Ding Fu supported the original manuscript's writing and performed the experimental validations. Haibo Wang provided crucial revisions to the final version and facilitated funding acquisition. Zhideng Zhou assisted in manuscript organization and revision.*

Acknowledgements *This work was supported by the National Natural Science Foundation of China (Grant No. 11802347), Guangdong Basic and Applied Basic Research Foundation (Grant Nos. 2018A030310334 and 2023A1515012482), and Guangzhou Basic and Applied Basic Research Foundation (Grant No. 2023A04J1618).*

1 Editorial Department of China Journal of Highway, Review on Chinas bridge engineering research·2014, China J. Highway Transport **27**, (2014).
2 L. P. Perera, and C. Guedes Soares, Collision risk detection and quantification in ship navigation with integrated bridge systems, Ocean Eng. **109**, 344 (2015).
3 Z. Fang, and Y. Ma, Investigation and consideration on ship collision accident of sea-crossing bridge in Chinese, China Water Transport **9**, 38 (2009).
4 J. Wang, and B. Geng, Probabilistic Risk Assessment and Measures of Ship-Bridge Collision in Chinese, 2010th Ed. (China Communications Press, Hongkong, 2010).
5 S. Wang, H. Ren, X. Yun, X. Yan, and D. Dan, Active early-warning system for bridge piers against ship collision and its performance analysis (in Chinese), China J. Highway Transport **25**, 94 (2012).
6 B. Ji, X. Gu, and Q. Gang, Study of AIS-based active collision prevention system for Su-Tong bridge, J. Navigation China **33**, 34 (2010).
7 W. Ma, Y. Zhu, M. Grifoll, G. Liu, and P. Zheng, Evaluation of the effectiveness of active and passive safety measures in preventing ship-bridge collision, Sensors **22**, 2857 (2022).
8 H. A. Tran, T. A. Johansen, and R. R. Negenborn, A collision avoidance algorithm with intention prediction for inland waterways ships, IFAC-PapersOnLine **56**, 4337 (2023).
9 J. Mei, J. Liu, M. Zhang, and W. Huang, Experimental and numerical study on the ballistic impact resistance of the CFRP sandwich panel with the X-frame cores, Int. J. Mech. Sci. **232**, 107649 (2022).
10 J. Mei, J. Liu, M. Zhang, Z. He, and W. Huang, Mechanical behaviors of the carbon fiber reinforced X-core sandwich structure under the dynamic compression, Compos. Struct. **303**, 116341 (2023).
11 S. Ehlers, K. Tabri, J. Romanoff, and P. Varsta, Numerical and experimental investigation on the collision resistance of the X-core structure, Ships Offshore Struct. **7**, 21 (2012).
12 X. G. Lian, L. X. Lu, and L. Pan, Investigation of energy absorption characteristics of circular paper tubes under axial impact loading, Int. J. Impact Eng. **165**, 104210 (2022).
13 L. Zhu, W. Liu, H. Fang, J. Chen, Y. Zhuang, and J. Han, Design and simulation of innovative foam-filled lattice composite bumper system for bridge protection in ship collisions, Compos. Part B-Eng. **157**, 24 (2019).
14 H. Fang, Y. Mao, W. Liu, L. Zhu, and B. Zhang, Manufacturing and evaluation of large-scale composite bumper system for bridge pier protection against ship collision, Compos. Struct. **158**, 187 (2016).
15 H. Tian, Analysis of collision protection performance of composite anti-collision devices for Lixinsha bridge in Guangzhou, Bridge Constr. **53**, 66 (2023).
16 J. Liu, and Y. Gu, Simulation of the whole process of ship-bridge collision, China Ocean Eng. **16**, 369 (2002).
17 J. J. Wang, Y. C. Song, W. Wang, and J. Li, Calibrations of numerical models by experimental impact tests using scaled steel boxes, Eng. Struct. **173**, 481 (2018).
18 P. Chen, and B. Sun, Simulation of crooked plate energy absorption structure under impact, Acta Mech. Sin. **38**, 521429 (2022).
19 Y. Wan, Y. Liu, C. Hu, J. Yao, F. Wang, and B. Yang, The failure mechanism of curved composite laminates subjected to low-velocity impact, Acta Mech. Sin. **39**, 423113 (2023).
20 K. Kan, Y. Xu, H. Xu, J. Feng, and Z. Yang, Vortex-induced energy loss of a mixed-flow waterjet pump under different operating conditions, Acta Mech. Sin. **39**, 323064 (2023).
21 C. Sun, Numerical Simulations of Ship Stopping Maneuver Using Overset Grid Technology, Dissertation for Doctoral Degree (Shanghai Jiao Tong University, Shanghai, 2020).
22 S. Rudan, I. Ćatipović, R. Berg, S. Völkner, and P. Prebeg, Numerical study on the consequences of different ship collision modelling techniques, Ships Offshore Struct. **14**, 387 (2019).
23 M. Song, J. Ma, and Y. Huang, Fluid-structure interaction analysis of ship-ship collisions, Mar. Struct. **55**, 121 (2017).
24 X. Ye, W. Fan, Y. Sha, X. Hua, Q. Wu, and Y. Ren, Fluid-structure in-

teraction analysis of oblique ship-bridge collisions, Eng. Struct. **274**, 115129 (2023).
25 X. Zhao, and C. Hu, Numerical and experimental study on a 2-D floating body under extreme wave conditions, Appl. Ocean Res. **35**, 1 (2012).
26 X. Hu, J. Zhong, L. Yang, X. Shen, Y. Chen, and Z. Yu, Influence of sacrificial pile on the navigation flow condition around bridge piers (in Chinese), Hydrodyn. Res. Prog. A **30**, 556 (2015).
27 Z. Zhan, Basic Research on Fatigue Strength of Common Structural Rules (CSR) for Container Ships, Dissertation for Doctoral Degree (Shanghai Jiao Tong University, Shanghai, 2013).
28 D. J. Guo, X. R. Bin, W. Z. Yu, Z. J. Feng, Z. Hai, and J. Y. Long, Calculation and analysis of water resistance of 30000t bulk carrier based on star-ccm+, Ship Sci. Technol. **45**, 34 (2023).
29 A. Derradji Aouat, and G. Earle, in Ship-structure collisions: Development of a numerical model for direct impact simulations: Proceedings of the International Offshore and Polar Engineering Conference, Honolulu, 2003.
30 G. R. Consolazio, and D. R. Cowan, Numerically efficient dynamic analysis of barge collisions with bridge piers, J. Struct. Eng. **131**, 1256 (2005).
31 B. Song, Numerical Simulation Study on Collosion Accidents Between Fishing Vessels and Bridge Piers, Dissertation for Doctoral Degree (Zhejiang Ocean University, Hangzhou, 2019).

一种新型高压水柱干扰桥船防撞方法的数值评估

陈进财, 魏锡泉, 黄菁菁, 符鼎, 王海波, 周志登

摘要 船撞桥事故在全球范围内都时有发生, 一旦发生造成的后果经常是灾难性的. 为此, 本文提出了一种新型高压水柱干扰防撞(HPWJI)方法, 与传统的通过防撞装置吸能来减缓船舶对桥梁撞击力的方法不同, 该方法主要是通过横向高压水柱冲击来直接或者间接改变船舶的航向, 使船舶偏离桥墩而不发生碰撞. 本文以中国沙湾河道为流域背景, 并运用ANSYS-FLUENT软件, 对一艘重约2000吨的船只在HPWJI方法下的航行情况进行了模拟分析. 模拟结果表明, HPWJI方法对船只的航行方向有较大的影响, 能够让船只偏离桥墩, 在理论上用于防止桥船碰撞是可行的; 船只的行驶速度越快, 船只在行驶一段位移时横向位移和偏转角越小, 其中船速小于7米/秒时水流对船舶运动路径产生的影响更为显著; 最后本文构建了船只横向位移与航速、纵向位移关系的模型公式, 该公式可用于预测不同航速下所选船只的最小安全距离(该距离时船只在HPWJI方法下刚好能偏离桥墩).